

Contract No:

This document was prepared in conjunction with work accomplished under Contract No. 89303321CEM000080 with the U.S. Department of Energy (DOE) Office of Environmental Management (EM).

Disclaimer:

This work was prepared under an agreement with and funded by the U.S. Government. Neither the U.S. Government or its employees, nor any of its contractors, subcontractors or their employees, makes any express or implied:

- 1) warranty or assumes any legal liability for the accuracy, completeness, or for the use or results of such use of any information, product, or process disclosed; or
- 2) representation that such use or results of such use would not infringe privately owned rights; or
- 3) endorsement or recommendation of any specifically identified commercial product, process, or service.

Any views and opinions of authors expressed in this work do not necessarily state or reflect those of the United States Government, or its contractors, or subcontractors.



Savannah River
National Laboratory®

A U.S. DEPARTMENT OF ENERGY NATIONAL LAB • SAVANNAH RIVER SITE • AIKEN, SC • USA

Measurement of Radiolytic Hydrogen Generation and Impact of Drying Treatments on Reactor-Exposed and Surrogate Aluminum Materials

C. G. Verst

A. L. d'Entremont

November 2021

SRNL-STI-2021-00625, Revision 0

SRNL.DOE.GOV

DISCLAIMER

This work was prepared under an agreement with and funded by the U.S. Government. Neither the U.S. Government or its employees, nor any of its contractors, subcontractors or their employees, makes any express or implied:

1. warranty or assumes any legal liability for the accuracy, completeness, or for the use or results of such use of any information, product, or process disclosed; or
2. representation that such use or results of such use would not infringe privately owned rights; or
3. endorsement or recommendation of any specifically identified commercial product, process, or service.

Any views and opinions of authors expressed in this work do not necessarily state or reflect those of the United States Government, or its contractors, or subcontractors.

Printed in the United States of America

**Prepared for
U.S. Department of Energy**

Keywords: *Gamma Radiolysis,
Dry Storage, ASNF*

Retention: *Varies*

Measurement of Radiolytic Hydrogen Generation and Impact of Drying Treatments on Reactor-Exposed and Surrogate Aluminum Materials

C. G. Verst
A. L. d'Entremont

November 2021

Savannah River National Laboratory is operated by
Battelle Savannah River Alliance for the U.S. Department
of Energy under Contract No. 89303321CEM000080.



REVIEWS AND APPROVALS

AUTHORS:

C. G. Verst, SRNL - Actinide Materials Science & Tech Date

A. L. d'Entremont, SRNL - Adv. Modeling & Simulation Date

TECHNICAL REVIEW:

C. L. Crawford, SRNL - Actinide Materials Science & Tech Date

G. P. Horne, Idaho National Laboratory Date

APPROVAL:

M. M. Reigel, Manager Date
Actinide Materials Science & Tech

J. J. Jarrell, Project Manager Date
Idaho National Laboratory

B. C. Randall, Project Manager Date
Savannah River National Laboratory

TABLE OF CONTENTS

LIST OF TABLES	vi
LIST OF FIGURES	vi
1.0 Introduction.....	1
2.0 Experimental Description	1
2.1 Glass Ampule Experiments.....	2
2.1.1 Sample Preparation.....	2
2.1.2 Flame Sealing	6
2.1.3 Ampule Irradiation.....	7
2.1.4 Gas Sampling and Gas Chromatography.....	7
2.2 Large Plate Experiments	8
2.2.1 Sample Preparation.....	9
2.2.2 Vessel Irradiation.....	12
2.2.3 Gas Sampling and Gas Chromatography.....	13
3.0 Results.....	13
3.1 Low Dose Ampule-Based Experimental Results	13
3.2 High Dose Ampule-Based Experimental Results.....	16
3.3 Large-Plate Experimental Results	21
4.0 Conclusion	22
5.0 References.....	25

LIST OF TABLES

Table 1. Reactor and wet storage history of the ASNf scrap material.5
Table 2. Cracking manifold volume.8
Table 3. Corroded *Low Dose* coupons.14
Table 4. Pristine *Low Dose* coupons.14
Table 5. Heated pristine *Low Dose* coupons.14
Table 6. Effect of vacuum hold time on radiolytic H₂ generation.15
Table 7. *High Dose* coupon results.17
Table 8. High Dose foil results.17
Table 9. *Large Plate* segment results.17
Table 10. ASNf scrap radiolysis results.20
Table 11. *As-Corroded* large plate results.21
Table 12. *As-Dried* large plate results.21

LIST OF FIGURES

Figure 1. *Low Dose* coupons being sheared.2
Figure 2. Parr vessels.3
Figure 3. *High Dose* coupons (left) and foils (right) before and after corrosion.4
Figure 4. SEM plan-view (top) and cross-sectional view (bottom) of the High Dose corroded coupons.4
Figure 5. Camera (bottom) and SEM cross-section (top) images of the segmented USH (left) and Mk16B (right) scrap.5
Figure 6. Schlenk lines used for clean (left) and contaminated (right) ample-based experiments.6
Figure 7. Model 109 gamma irradiator.7
Figure 8. Ample cracking and gas sampling manifold.7
Figure 9. H₂ concentration calibration for GC.8
Figure 10. As-Corroded plate assembly during and after room temperature water submersion for 41 days.9
Figure 11. Water bubble forming on at the exhaust of the vessel during drying.10
Figure 12. SEM cross-section images of the *As-Corroded* oxide layer, 5-10 μm thick.11
Figure 13. Examples of (oxy)hydroxide morphology from *As-Corroded* (left) and *As-Dried* (right) large-coupon assemblies. Several fine cracks in the *As-Dried* (oxy)hydroxide are marked with red ovals in the enlarged section at top right.11
Figure 14. XRD spectra of the *As-Corroded* (top) and *As-Dried* plate assembly surfaces.12
Figure 15. Model 484 gamma irradiator (left), a top-down dose rate profile generated from an MCNP model of the vessels containing plate assemblies (mid), and large plate vessels loaded into irradiation chamber (right).13
Figure 16. Plot of *Low Dose* coupon H₂ measurements.14
Figure 17. Total moles of H₂ generated as a function of absorbed dose and drying temperature.18
Figure 18. Moles of H₂ generated per gram of corrosion weight gain as a function of absorbed dose and drying temperature.19
Figure 19. Sealed ampules containing ASNf Scrap pieces. From left to right, USH1, USH2, Mk16B1, Mk16B2, argon blank.20
Figure 20. Moles of H₂ generated at 0.8 MGy for ASNf scrap as a function of drying temperature.20
Figure 21. H₂ yields from As-Corroded and As-Dried large-plate assemblies.22

1.0 Introduction

Technical challenges associated with dry storage of Aluminum-clad Spent Nuclear Fuel (ASNF) include a need to better understand the potential extent of gaseous molecular hydrogen (H_2) production through radiolytic degradation of the aluminum (oxy)hydroxide films present on ASNF. The characterization of radiolytic gas generation from ASNF (oxy)hydroxide layers has been identified as a key knowledge gap which poses a technical challenge to the long-term storage of ASNF [1]. Task 2 of the action plan for the extended (>50 years) dry storage of ASNF addresses this gap [2].

Previous radiolysis studies performed under Task 2 established baseline estimates of H_2 generation rates from the attendant hydrated oxides [3]. The results confirmed that net radiolytic H_2 production has a dependency on absorbed gamma dose, as well as relative humidity and cover gas composition (air, nitrogen, and argon). Further experiments revealed that the physisorbed water on the samples may significantly impact the radiolytic H_2 yield. This phenomenon complicates the determination of H_2 generation rates for hydrated oxides, which may lead to inaccurate modeling predictions of the long-term H_2 yields in sealed storage systems containing ASNF, particularly when compared to spent fuel casks which have undergone some drying process intended to remove physically- and chemically-bound water.

This report describes the testing methods utilized and the hydrogen generation results obtained in an investigation of the effects of gamma irradiation on aluminum materials for a variety of (oxy)hydroxide surface compositions and drying conditions. The testing methods included small-area aluminum material testing in ampules, and large-area aluminum material testing in steel vessels. Test material preparation, irradiation, and radiolytic H_2 measurement methods are summarized. The measured H_2 concentrations, which reflect the variable initial hydrated inventory and drying treatments, are compared to one another as well as to previously published data, to identify the primary factors affecting radiolytic H_2 generation rates and potential equilibrium H_2 concentrations.

2.0 Experimental Description

The experiments described herein involve exposure of corroded aluminum materials, with a hydrated oxide surface formed by submersion in water, to a gamma field while sealed in an inert container and quantification of the radiolytic H_2 produced. This document covers several independent and joint experiments which can be subdivided into two fundamental sealed system types: glass ampules and steel vacuum vessels. The glass ampule work utilized small volume, flame-sealed glass ampules to contain corroded and pristine aluminum coupons. The irradiated glass ampules were crushed to release the accumulated H_2 for quantification by gas chromatography (GC). The benefit and initial driving factor for using glass ampules for this work was to eliminate any sources of radiolytic gas generation from interaction of radiation and/or radiolytic species with the materials comprising the steel vacuum vessels. However, the glass ampule approach limits data collection, as only one data point can be obtained from each prepared and irradiated sample.

Steel vacuum vessels with copper gaskets were eventually determined to be a viable alternative to the glass ampule method through multiple demonstration of zero net H_2 production from irradiated sealed vessels containing He gas but no metal samples. These vessels allowed the housing of much larger sample sizes, resulting in a quicker net production of quantifiable H_2 , despite the lower gamma dose rates due to self-shielding and flux falloff associated with increased distance between the larger samples and the Co-60 source. Further, the ample headspace of these steel vessels allowed repeat sampling at multiple dose points. The following sections detail both the glass ampule and steel vacuum vessel experimental setups along with characterization of the various aluminum samples irradiated within.

2.1 Glass Ampule Experiments

Glass ampule experiments comprised the bulk of the radiolysis testing performed at Savannah River National Laboratory (SRNL) and generally consist of small aluminum coupons with a known hydrated aluminum oxide surface layer, produced either through laboratory or service-induced corrosion processes, irradiated within a sealed glass ampule containing dry argon cover gas. Ampule-based experiments can be further partitioned into three categories based on their sample origin and intended objectives: “*Low Dose*”, “*High Dose*”, and “*ASNF Scrap*”.

The *Low Dose* experiments served as the proof of concept for ampule-based radiolysis experiments of lab-grown corrosion layers and yielded net H₂ generation rates as a function of dose between 0 and 0.7 MGy. These experiments also provided bounding confirmation of results from complementary Task 2 experiments performed by the Idaho National Laboratory (INL) Center for Radiation Chemistry Research (CR2) for alternate corrosion and dose rate conditions. *Low Dose* tests also included preliminary testing of the impact of thermal and vacuum drying on H₂ yield.

The *High Dose* experiments at SRNL involved long-term exposures from 0.7 MGy to 1.8 MGy of lab-corroded coupons and foils to evaluate the impact of sample surface area and various pre-irradiation thermal treatments for the removal of physi- and chemisorbed water. Attempts were made to quantify and differentiate between physi- and chemisorbed water through thermogravimetric analysis (TGA), but the relative water mass loss proved too low to be accurately measured for such thick aluminum materials and thus the physisorbed water present and removed for a drying process could not be quantified.

The testing of pre-irradiation drying treatments was intended to evaluate the benefits of a proposed spent fuel drying process in terms of hydrogen generation under attendant radiation of the fuel. The *High Dose* experiments also investigated, to a limited degree, the correlation between irradiated ASNF surface area and equilibrium H₂ concentrations in a finite, non-reactive, cover gas volume.

The *ASNF Scrap* experiments utilized pieces of actual reactor-exposed aluminum scrap segmented from ASNF and irradiated reactor components to provide the first comparison of lab-grown radiolysis samples to actual service-induced radiolytic sources akin to the material which would actually be stored in ASNF dry storage systems. Like the *High Dose* coupons, these ASNF scrap samples were also thermally pre-treated at different temperatures to evaluate the impact of drying on radiolytic H₂ production. All *ASNF Scrap* was irradiated to 0.8 MGy.

2.1.1 *Sample Preparation*

Low Dose coupons were segmented sections sheared from a larger 1/16” (0.0625”) thick aluminum alloy 1100 (AA1100) disc specimen purchased from Metals Samples Company – Alabama Specialty Products Inc. with a 600-grit vendor finish. Segmented coupons were manually sheared to approximately 1” L x 0.25” W and were engraved with unique IDs. The effect of surface cleaning (e.g., sequential sonication in acetone, ethanol, and distilled water) on hydrogen generation rates was investigated with early *Low Dose* samples, but the effect was determined to be insignificant, and the treatment was considered atypical of service-induced corrosion of ASNF and therefore waived for the experiments reported in this document.



Figure 1. *Low Dose* coupons being sheared.

High Dose aluminum samples were similarly AA1100 ordered from Alabama Specialty Products Inc. but were pre-cut to exactly 1.5" L x 0.25" W. Two thicknesses were procured: 1/16" coupons and 0.01" foils. A surface finish was not available for the foil, so it was not requested for the coupons to ensure comparable surface conditions among *High Dose* samples, although it meant diverging from earlier 600-grit vendor finish *Low Dose* samples. As discussed later, results suggest that the surface finish did not significantly impact the H₂ generation rates nor equilibrium concentrations.

Both the *Low Dose* and *High Dose* coupons' masses were recorded before undergoing a high-temperature water submersion to induce corrosion and promote development of hydrated aluminum oxide. The hydrated oxide targeted for this scope was boehmite, which forms preferentially at higher water temperatures compared to other morphologies such as gibbsite or bayerite [4]. Boehmite was selected to complement radiolysis experiments conducted by INL in which lab-induced corrosion of aluminum coupons was performed in 95 °C water. This process took 29 days to produce a ~5 μm mixed oxide layer of predominantly bayerite favored by lower water temperatures [3]. Conversely, SRNL efforts focused on the high-temperature crystalline boehmite which is expected to be the dominant form of hydrated oxyhydroxide after undergoing most fuel drying processes, as the elevated temperatures employed would transition gibbsite or bayerite into boehmite [5]. Boehmite has also been observed on aluminum coupons exposed to lower water temperature (<50 °C) for a period up to 1 year [6].

Corrosion of the *Low Dose* and *High Dose* coupons was performed in distilled water at 185 °C using small model 4749 Parr vessels, **Figure 2**. Single coupons, or 8 foils, were loaded into a 23 mL polytetrafluoroethylene cup filled with 15 mL of distilled water and then sealed within one of four available Parr vessels via screw threads between the cap and vessel. The sealed vessels were then loaded into an oven pre-heated to 185 °C and left for 18 hours. The Parr vessels were then removed and allowed to cool for 2 hours at ambient temperature prior to removing the corroded coupons, which were then set aside to air dry overnight before being re-weighed and sealed for irradiation. This corrosion process was performed in batches of four Parr vessels. Recorded weights reflect measurements taken immediately preceding each step.



Figure 2. Parr vessels.

As anticipated, the 185 °C water submersion treatment of the AA1100 coupons resulted in a thin layer of crystalline boehmite deposited on the surface, as confirmed by X-ray diffraction (XRD) and scanning electron microscopy (SEM) techniques. XRD was performed using a Bruker D8 Advance utilizing a copper x-ray source, and SEM was performed using a Carl Zeiss Microscopy LLC Sigma VP field emission scanning electron microscope. The boehmite layer on corroded coupons was generally only 1-2 μm thick with sporadic regions of up to 10 μm thick, as determined by cross-sectional SEM. Average weight gain after corrosion and air drying was 5 mg/cm² for the 1/16" thick coupons and 3.3 mg/cm² for the 0.01" thick foils. An image of the coupons and foils before and after corrosion is given in **Figure 3**, where it can be seen that the original aluminum sheen has faded to a dull matte gray due to the presence of the oxyhydroxide after corrosion. SEM plan- and cross-sectional views of the aluminum coupons corroded in this way are given in **Figure 4**.

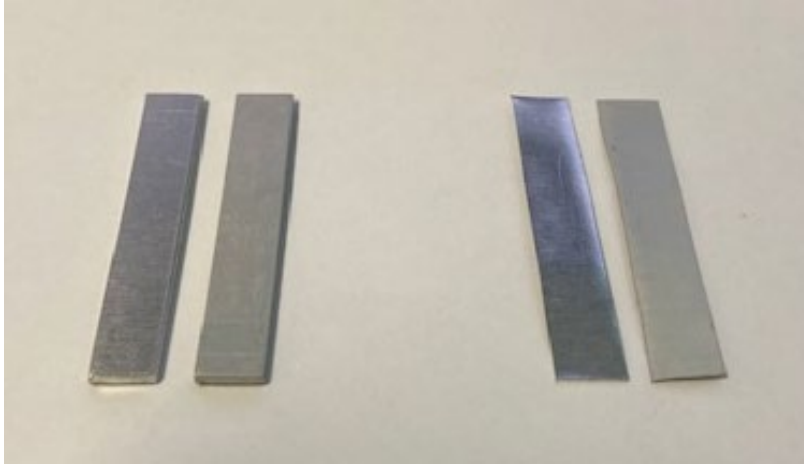


Figure 3. *High Dose* coupons (left) and foils (right) before and after corrosion.

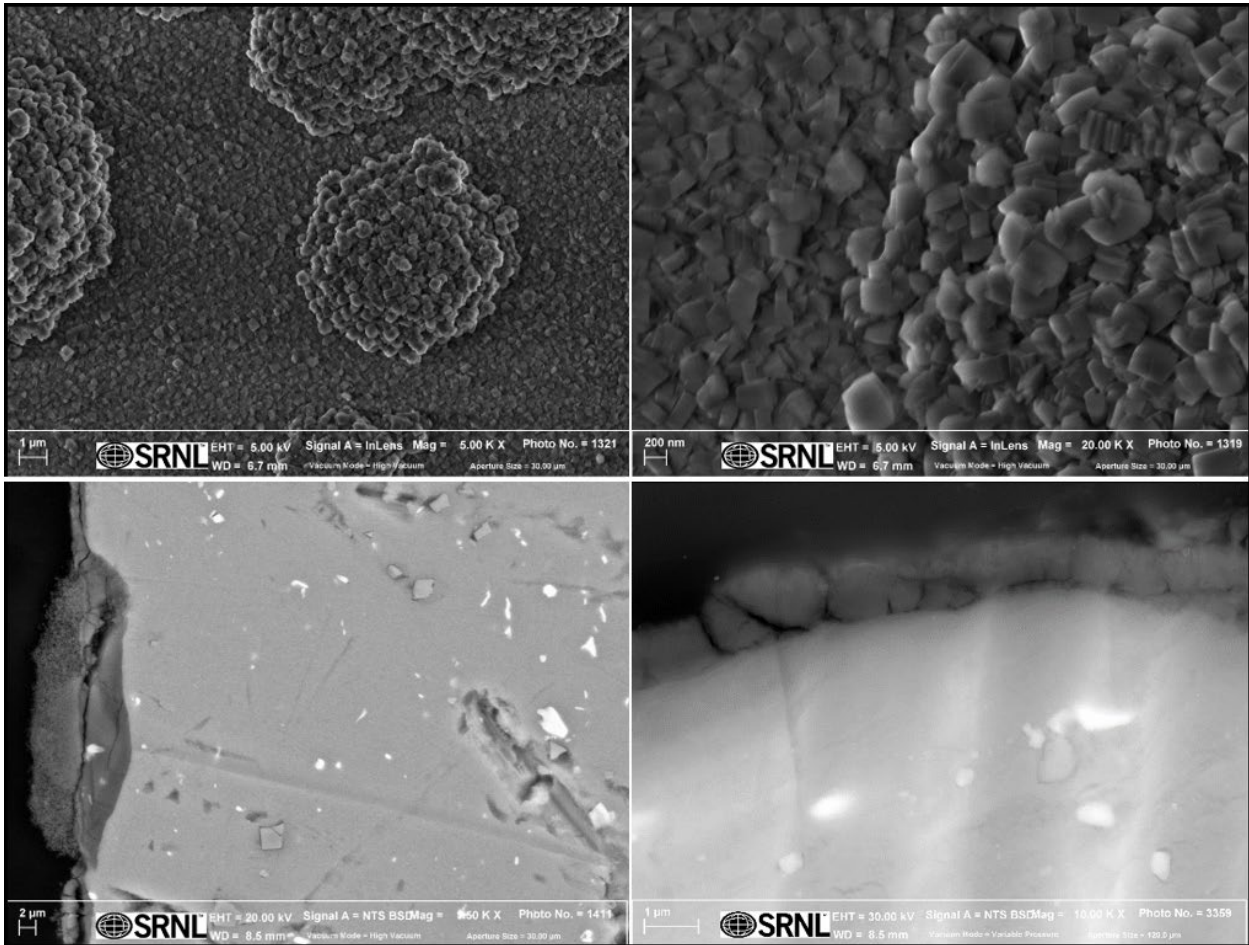


Figure 4. SEM plan-view (top) and cross-sectional view (bottom) of the *High Dose* corroded coupons.

The *ASNf Scrap* material was segmented from two distinct aluminum components which were stored in the L Basin spent fuel storage facility after being exposed in various reactors during their service life. The two croppings are from a Universal Sleeve Housing (USH) and a Mark-16B (Mk16B) assembly. The in-reactor operation and post-discharge storage history are provided in **Table 1**.

Table 1. Reactor and wet storage history of the ASNF scrap material.

Cropping	Min. Operation Temperature [°C]	Operations Time [days]	Storage Temperature [°C]	Storage Time [years]
USH	38-93	~1800	22	~40
Mk16B	38	~220	22	~40

The surface (oxy)hydroxide layers of each of these croppings were extensively characterized previously [7]. The USH yielded a stronger boehmite XRD signal than the Mk16B, consistent with its higher expected operating temperature (up to 93 °C [7]), and both USH and Mk16B had XRD peaks for bayerite. However, cross-sectional SEM could not discern a visible oxide layer on the USH which suggests that the layer is very small (<1 μm) or was accidentally removed during sample preparation. The Mk16B cropping, believed to have operated in a colder environment near the 38 °C coolant inlet region of the reactor [7], also had XRD peaks for gibbsite, though they were dwarfed by the bayerite signal. The oxyhydroxide layer of the Mk16B was reported to be relatively uniform with an average thickness of 10 μm across the majority of the characterized area, as determined by cross-sectional SEM. However, localized areas of extensive pitting were observed and included in the sample matrix of this radiolysis work. Images of the segmented scrap and their corresponding SEM cross-sections are given in **Figure 5**.

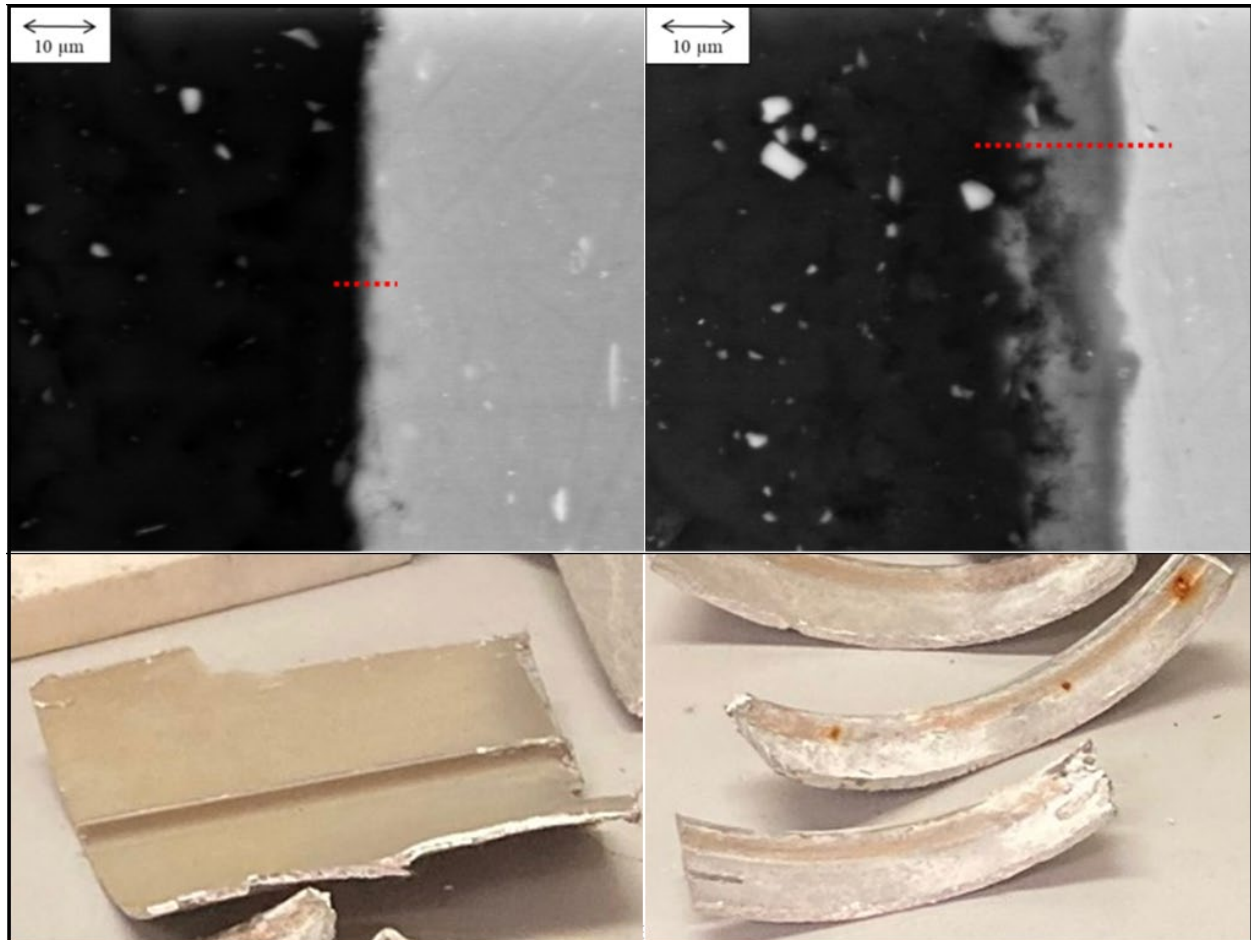


Figure 5. Camera (bottom) and SEM cross-section (top) images of the segmented USH (left) and Mk16B (right) scrap.

For each aluminum coupon irradiated in the ampule-based experiments, a single glass vial (10 mm outer diameter and 8 mm inner diameter) would serve as the sealed system's container, with the vial length determined by the location of flame-sealing. Each vial was initially baked out to drive off any adhered moisture prior to loading any coupons. To perform this step, vials were loaded into larger glass tubes and placed in a furnace set to 350 °C overnight (>16 hr). Once it was time to load coupons into the vials, the vials were removed from the furnace, and their outer glass tubes were capped to prevent ambient air ingress while the vials cooled. Coupons would only be loaded into the vials immediately before the vial was connected to a Schlenk line under an argon purge. Coupons and *ASNF Scrap* material that underwent high-temperature pre-irradiation thermal treatments were similarly heated in glass overpack tubes, which were sealed during cooling and transportation to minimize any potential re-wetting of the dried coupons surface.

2.1.2 Flame Sealing

A Schlenk line was used to ensure a pure argon atmosphere in each ampule containing oxidized aluminum samples. The line was connected to a supply of ultra-high purity (UHP) (i.e., >99.999%) argon and allowed to purge for several minutes before the loaded ampules were connected. Batches of 5-6 vials were sealed onto the line via plastic tubing and hose clamps (later upgraded to gasketed Teflon fittings). Each batch included at least one blank vial containing no aluminum sample, which, once sealed, was analyzed by GC to confirm a pure argon atmosphere. The desired atmosphere was obtained by cycling between a vacuum hold of 15 mtorr followed by an argon purge, with each step lasting approximately 30 seconds. This sequence was repeated 3 times, at which point the vacuum was valved off and the line exhaust through a water manometer left open to allow thermally expanded gas to exit during the flame sealing step. A propane torch was used to seal the vials at a length of 85 mm from the bottom, resulting in consistent ampule lengths/volumes containing oxidized aluminum samples in pure argon at slightly less than atmospheric pressure. Internal volumes were calculated to be in the range 3.6-3.8 mL, depending on the size of the aluminum coupon within. Images of the Schlenk lines used for the clean (*Low Dose* and *High Dose*) and contaminated (*ASNF Scrap*) sample work are shown in **Figure 6**.



Figure 6. Schlenk lines used for clean (left) and contaminated (right) ampule-based experiments.

2.1.3 Ampule Irradiation

Gamma irradiations were performed using a J. L. Shepherd Model 109-68R Co-60 gamma irradiator unit. This unit features 16 pencil sources of cobalt-60 (Co-60) situated in a ring around the central irradiation chamber to provide a highly uniform dose rate profile. Dosimetry for the unit was determined by Fricke solution in 1995, and subsequently corrected for the decay of Co-60. The resulting dose rates were further confirmed in January 2020 through NIST traceable, calibrated ion chamber measurements at multiple locations within the irradiation chamber. The dose rates for radiolysis samples covered in this work ranged from 10 Gy/min in 2019 to 7.5 Gy/min in 2021. Due to the symmetry of the dose profile in the unit and the negligible amount of dose attenuation expected from the thin ampules and aluminum itself, no further shielding correction factors are included in the reported dose rates.



Figure 7. Model 109 gamma irradiator.

2.1.4 Gas Sampling and Gas Chromatography

Following irradiation, the ampules containing the irradiated aluminum samples were loaded into a custom cracking manifold designed to shatter the ampule and contain the radiolytically generated gases in a known volume to equilibrate before being sampled by the GC. The cracking manifold consists of a steel sanitary flange sealed with a rubber reusable gasket and C-clamp. The manifold features a UHP argon gas inlet, matching the composition of the GC carrier gas, a meter valve to a water manometer exhaust, a pressure transducer, a screw-threaded impinging arm used to crack the ampule within, and an exhaust line into the GC. Ampules are loaded into one half of the sanitary flange, which is then sealed with the other half. Argon gas is then purged through the device and out of the primary exhaust leg, while the GC collects gas from the secondary exhaust leg. Once the GC indicates no remaining air in the manifold, the primary exhaust valve is closed, and the manifold is slightly pressurized to 22 psia. This pressurization is needed to overcome the GC's non-linear response at sample inlet pressures near and below atmospheric. Images of a loaded sanitary flange and assembled cracking manifold are shown in **Figure 8**.



Figure 8. Ampule cracking and gas sampling manifold.

The GC used for the ampule-based radiolysis experiments was an Inficon model 3000 microGC equipped with a thermal conductivity detector (TCD) and a 10 m long molecular sieve column. When triggered, the operating software was programmed to pull 4 consecutive gas samples from the cracking manifold. The first sample was discarded as it would be diluted by the plug of purge gas in the capillary line through which the

sample could not quickly diffuse. The resulting TCD plots yield the relative concentrations of detectable gas species in the sample. GC calibration was performed by direct injection of 50 and 100 ppm H₂ gas standards. The ideal gas law was used to determine the number of moles of H₂ produced in each ampule. This required the volume and pressure of gas in the cracking manifold after the ampule is shattered to be known. The volume was determined through measured pressure changes in the manifold upon injection of an additional known gas volume using the following equation:

$$V_{manifold} = \frac{V_{inject} \times P_{inject}}{P_{man_{pre-inject}} - P_{man_{post-inject}}}$$

The calibration curve for the GC is given in **Figure 9** and the results of the calculated cracking manifold are given in **Table 2**.

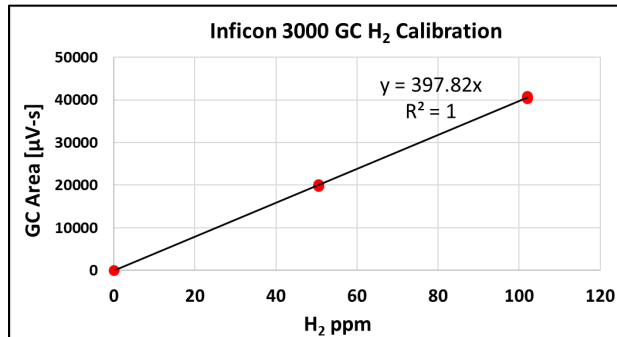


Figure 9. H₂ concentration calibration for GC.

Table 2. Cracking manifold volume.

Pre-Inj. Press. [psia]	Post-Inj. Press. [psia]	Inject Press. [psia]	Inject Vol. [mL]	Calc. Manifold Volume [mL]
14.5	17.6	14.5	10	46.77
14.5	19.16	14.5	15	46.67
14.5	20.74	14.5	20	46.47
14.5	22.24	14.5	25	46.83
18	21.08	14.5	10	47.08
Average Calculated Manifold Volume:				46.77

2.2 Large Plate Experiments

Following the early success of the small-scale, glass-ampule-based radiolysis experiments, attention was directed towards bench top surrogates for dry cask storage systems. Baseline radiolysis testing was performed on steel vacuum vessels with copper gasket closures containing pure helium to ensure that surface moisture on the vessel walls would not contribute to radiolytic H₂ generation and that leak tightness could be maintained for long duration irradiations. The vessel was placed in an irradiator and featured a 6 ft long steel capillary line connecting it to a gas sampling manifold from which samples could be analyzed by GC. All valves associated with the manifold were external to the radiation field to avoid any radiolysis of their components. An atmosphere of helium was created in the sealed vessel through successive evacuation and backfill cycles. Intermittent gas sampling of the sealed vessel atmosphere showed no detectable H₂ during the course of a 24-day irradiation period, corresponding to a dose of ~0.3 MGy. Minimal (~10 ppm) air concentrations were detected in the vessel 1 day after being sealed with the helium atmosphere, but these measurements stayed consistent throughout the full irradiation period and were attributed to air that was still present in the vessel on day 0 that had not yet equilibrated through the 1/16" capillary line until after the first measurement was taken.

Use of larger steel vacuum vessels, compared to one-time-use glass ampules, provided the benefit of sequential sampling of the same hydrated aluminum material, thereby eliminating some of the experimental noise caused by variations in the physi- and chemisorbed water inventory shown to exist between individual coupon samples which undergo nominally identical corrosion procedures. Furthermore, the larger working volume of the vessels allowed for maximization of the aluminum surface area and therefore (oxy)hydroxide and adhered moisture inventory within the sealed volume by use of several thin aluminum plates. This provided a suitable facsimile for the Materials Testing Reactor (MTR) plate fuel stored in a dry cask storage system.

2.2.1 Sample Preparation

Two large-plate assemblies were fabricated from 17 individual aluminum 6061T6 plates per assembly, each 0.050" thick, bolted together with aluminum hardware, and separated from each other by aluminum washers to provide a 2 mm plate pitch. The plate height and widths were cut to maximize the plate area in the steel vessel, resulting in an aluminum surface area of nearly 3800 cm². The plates were polished to 600 grit and rinsed with distilled water immediately prior to being assembled and then immersed in room-temperature distilled water to undergo the prescribed corrosion treatment. This low-temperature immersion was expected to produce a bayerite (trihydroxide) film, in contrast to the boehmite film produced at high temperature on the coupons for glass-ampule-based tests. The first assembly remained in the water bath maintained between 22 °C and 23 °C for 41 days and was then air-dried for 7 days prior to being weighed to determine a corrosion product mass gain of 5.5 g, or 0.90%. The second assembly was prepared and corroded in the same fashion for 36 days, and gained 5.3 g, or 0.87%.

Small sections were cut from an external plate from each assembly for XRD and SEM characterization as well as for use in confirmatory glass-ampule-based experiments. An image of one of the assemblies being corroded is provided in **Figure 10**, during which bubbles, presumed to be H₂ from the corrosion reaction, can be seen forming and rising through the water. Also shown is the plate assembly after it was corroded and loaded into the steel vacuum vessel.

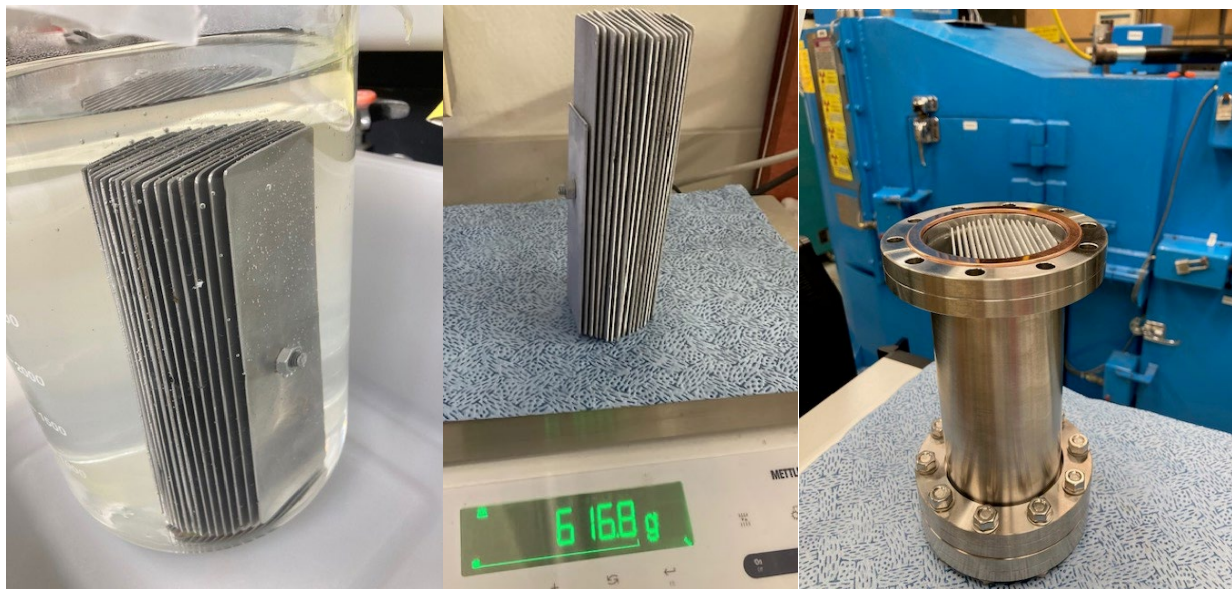


Figure 10. As-Corroded plate assembly during and after room temperature water submersion for 41 days.

The second plate assembly underwent a thermal drying step once it was sealed within the bolted-closure steel vessel for the purpose of illustrating potential impacts of fuel drying on the radiolytic H₂ yields in a dry cask storage system. This large-plate assembly is termed the “*As-Dried*” assembly while the first plate assembly which did not undergo any thermal drying steps is referred to as the “*As-Corroded*” assembly. The loaded vessel for the *As-Dried* assembly was placed in a pre-heated oven at 220 °C for 4 hours with the valved end of the capillary sample line open to allow moisture to escape. **Figure 11** depicts a bubble forming on the exhaust of the *As-Dried* vessel, suggesting the removal of significant moisture and, correspondingly, significant moisture remaining in the *As-Corroded* vessel. Following the 4-hour heating period, the oven was turned off and the *As-Dried* vessel’s exhaust line was connected to a vacuum pump for 1 hour while it remained in the residual oven heat. This step ensured that any steam would be removed from the vessel and capillary line before recondensing as the vessel cooled to room temperature. The plate segment removed from the *As-Dried* assembly after corrosion was placed in the furnace next to the mini canister, so that it experienced the same heat treatment (albeit not vacuum treatment) as the corresponding assembly.



Figure 11. Water bubble forming on at the exhaust of the vessel during drying.

At this point, both the *As-Corroded* and *As-Dried* vessels were connected to a gas sampling manifold through which dry, UHP helium was provided. An initial overnight vacuum was performed on both vessels, followed by a series of vacuum/purge cycles to ensure a pure helium atmosphere within. Vessels were finally sealed with a helium pressure of ~24 psia and positioned symmetrically in a Co-60 irradiator to begin the radiolysis experiment.

Cross-sectional SEM characterization of the large-plate sections taken from the *As-Corroded* plate segment indicated a relatively consistent (oxy)hydroxide layer measuring 5-10 μm thick, **Figure 12**. Plan-view SEM of the *As-Corroded* and *As-Dried* large-coupon sections show near-identical (oxy)hydroxide morphology, **Figure 13**, which appears to consist predominantly of long narrow rods of (oxy)hydroxide. In some regions, these rodlike structures form “bundles” of parallel rods which project out from the substrate at various angles. In other areas, the surface of the oxide consists of shorter, individual rods in seemingly random orientations. The areas dominated by randomly oriented rods appear to be the highest points on the (oxy)hydroxide layer and some appear to have “bundles” of aligned rods projecting out from under the edges of the randomly oriented patches, suggesting that the randomly oriented rods may be a surface layer sitting on top of the structures of aligned rods.

Image comparisons of the two plates revealed the presence of narrow cracks in the *As-Dried* (oxy)hydroxide. The cracks are visible in several areas that are dominated by the aligned-rod structures, running roughly perpendicular to the direction of the aligned rods. The crack width is on the order of 0.1 μm, i.e., of similar scale to the width of the isolated (oxy)hydroxide rods, which would make the cracks very difficult to visually distinguish in the disordered regions, if present.

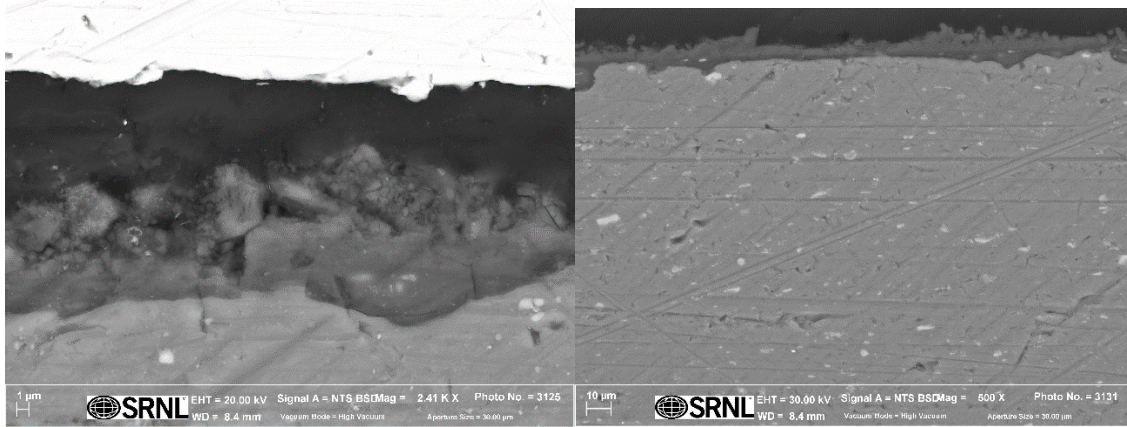


Figure 12. SEM cross-section images of the *As-Corroded* oxide layer, 5-10 μm thick.

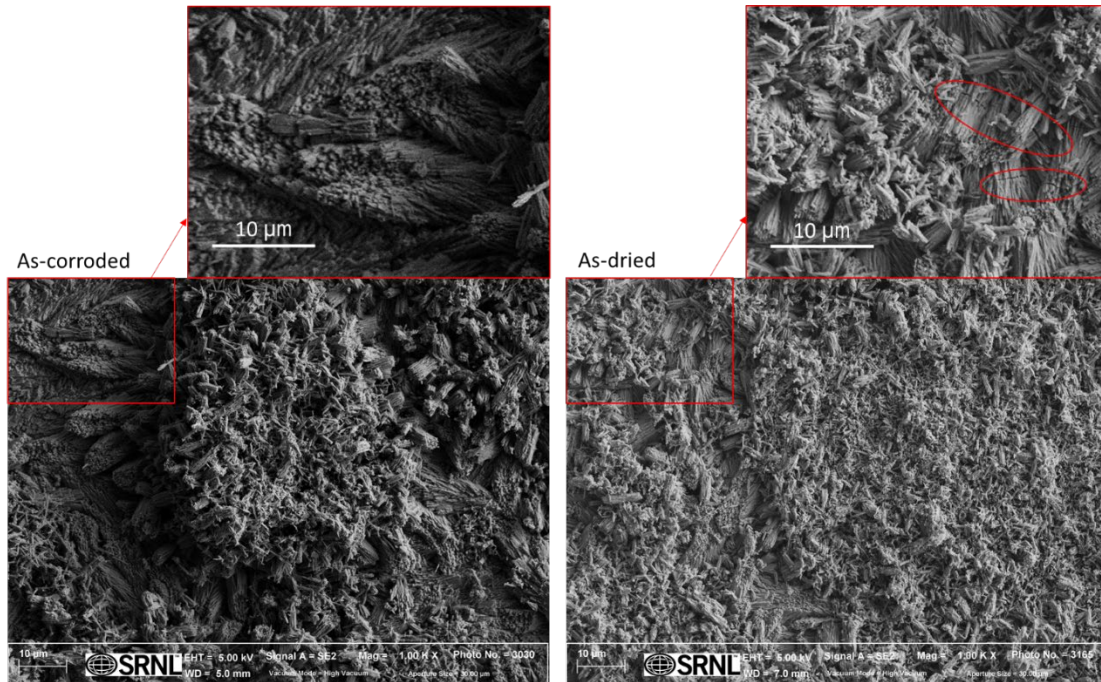


Figure 13. Examples of (oxy)hydroxide morphology from *As-Corroded* (left) and *As-Dried* (right) large-coupon assemblies. Several fine cracks in the *As-Dried* (oxy)hydroxide are marked with red ovals in the enlarged section at top right.

The XRD spectrum for the *As-Corroded* large-coupon assembly (Figure 14, top) shows prominent, sharp peaks for bayerite as well as for aluminum metal, along with a small, broad peak corresponding to boehmite. Post-drying (Figure 14, bottom), bayerite remains the most prominent oxyhydroxide signal, but clear, sharp boehmite peaks are also present. The height of the bayerite peaks relative to the aluminum peaks is smaller for the *As-Dried* sample compared to *As-Corroded*. The reduction in bayerite peaks and appearance of distinct boehmite peaks suggests that the 220 °C, 4-hour drying process was successful in partially converting the bayerite to well-crystallized boehmite. No corundum peaks were identified, as expected since thermal decomposition of boehmite to alumina is associated with higher temperatures.

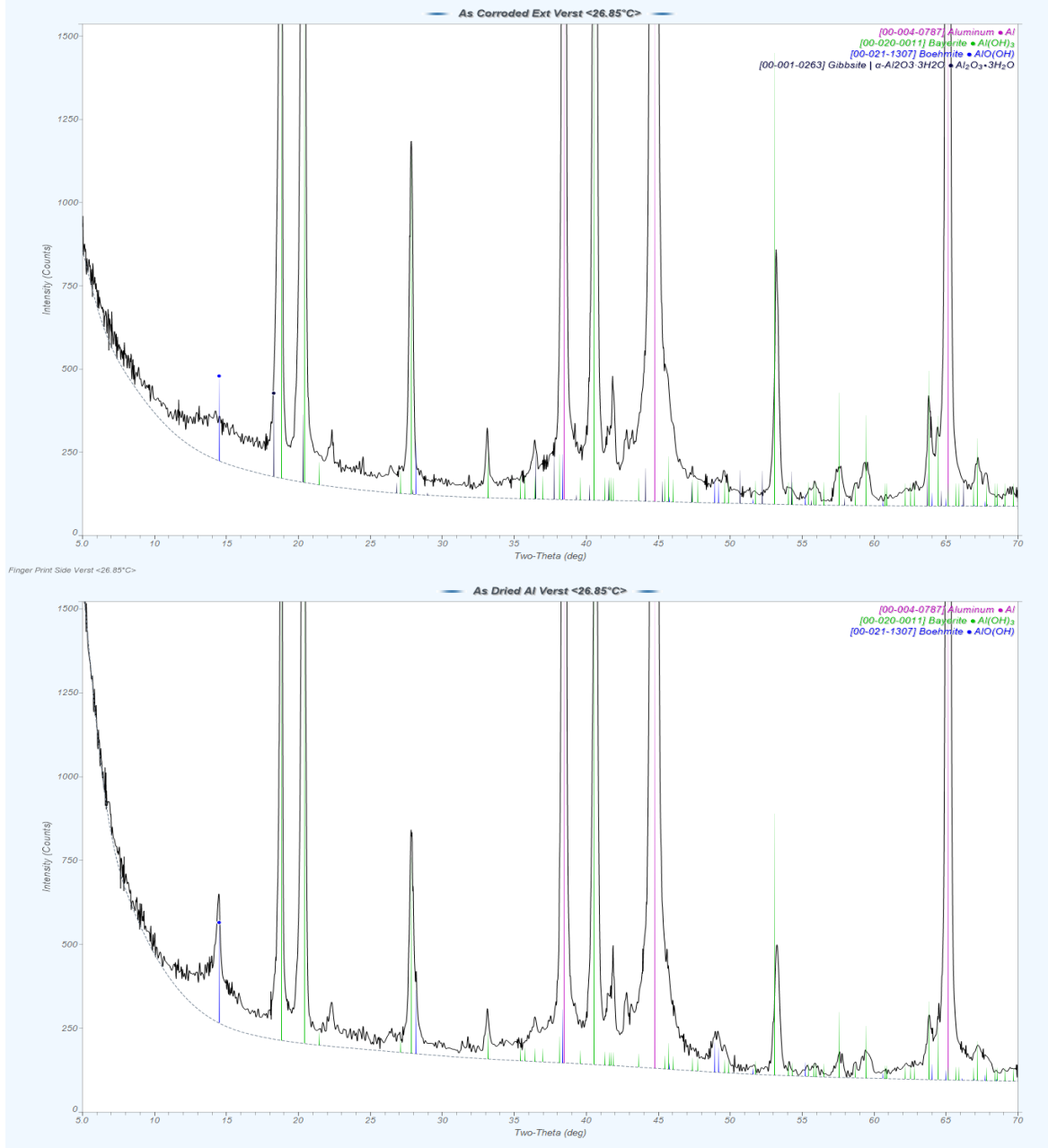


Figure 14. XRD spectra of the *As-Corroded* (top) and *As-Dried* plate assembly surfaces.

2.2.2 Vessel Irradiation

Gamma irradiation of the vessels containing *As-Corroded* and *As-Dried* plate assemblies was performed using a J. L. Shepherd model 484 Co-60 gamma irradiator. The irradiator features two Co-60 pencil sources at one end of the irradiation chamber. The vessels were placed symmetrically adjacent to each pencil source as close as could be achieved. Due to the proximity of the sample volume to the Co-60 sources, dose rates across the plate assembly could vary by as much as $\pm 40\%$. However, radiation transport modeling of the configuration using Monte Carlo N-Particle (MCNP) determined orientation of the plates within the vessels would not impact the volume-averaged dose rates, and due the symmetric position of the two vessels it was determined that a single volumetric-average dose rate value could be ascribed to both plate assemblies. The reported dosimetry for the plates was therefore measured by a single Fricke solution irradiated within an

empty vessel at one of the symmetric locations. The Fricke solution yielded a decay-corrected dose rate of 6.3 Gy/min at the irradiation start date of the *As-Corroded* plate assembly, and a dose rate of 6.2 Gy/min at the irradiation start date of the *As-Dried* plate assembly. Despite the variation in dose rate across the plate assembly surface, the *As-Dried* and *As-Corroded* assemblies feature the same dose rate profile, and so can be compared against each other. Furthermore, joint INL and SRNL experiments have demonstrated that the H₂ G-value from similar aluminum radiolysis experiments is not strongly dependent on dose rate between 8 Gy/min and 175 Gy/min [8]. However, because it is yet unknown whether depletion of the water inventory may lead to an appreciable reduction in H₂ generation rates in areas that experience very high total absorbed doses, caution should be used when comparing these radiolysis data to other experiments, as the reported H₂ concentrations correspond to the total yield while the local yield might vary spatially across the assembly surface due to varying dose rate and levels of water depletion.

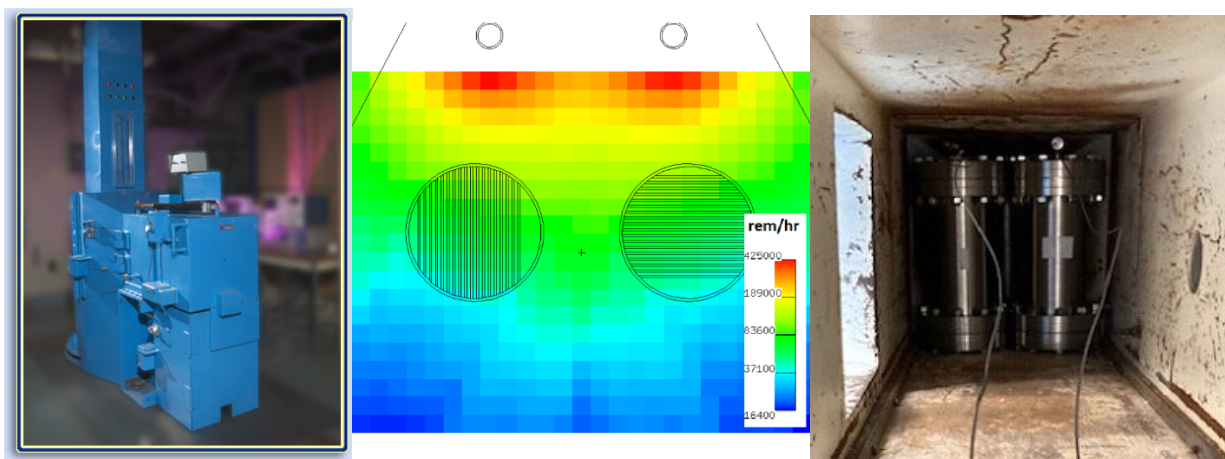


Figure 15. Model 484 gamma irradiator (left), a top-down dose rate profile generated from an MCNP model of the vessels containing plate assemblies (mid), and large plate vessels loaded into irradiation chamber (right).

2.2.3 Gas Sampling and Gas Chromatography

A gas sampling manifold was used to collect 10 mL aliquots from each irradiated vessel at semi-regular intervals. The pressure of the vessel was recorded after each aliquot was removed and the gas was automatically injected into an Inficon Micro GC Fusion Gas analyzer equipped with a TCD sensor and two analytical columns. The primary GC column was a 20 m molecular sieve utilizing an argon carrier gas designated to quantify H₂ concentrations. The secondary column was a shorter, 10 m molecular-sieve column with a helium carrier gas, primarily used to quantify oxygen and nitrogen. GC calibration was performed using direct injection of 260/251/946, 510/510/1924, and 5018/4946/18661 ppm H₂/O₂/N₂ in a balance of He. A vacuum pump was used to evacuate the sampling manifold between aliquots. Because each sample taken permanently reduces the gas inventory remaining in the vessel, the total radiolytic H₂ generation calculation was corrected for the moles of H₂ in previous aliquots and for changing vessel pressure.

3.0 Results

3.1 Low Dose Ampule-Based Experimental Results

The results of the low-dose, ampule-based experiments are given in **Tables 3-5** and plotted in **Figure 16**. These ampules contained AA1100 of slightly varying sizes that were either pristine (as received from the vendor with a 600 grit finish) or corroded via water submersion at 185 °C for 18 hours to produce a boehmite

film prior to overnight air drying. All coupons were flame-sealed in glass ampoules containing dry argon atmospheres.

Table 3. Corroded *Low Dose* coupons.

Coupon ID	Dose [Gy]	Weight Gain [g]	Mols H ₂ Generated
116	2.53E+04	0.0017	1.12E-08
117	2.53E+04	0.0013	1.53E-08
118	5.54E+04	0.0014	2.81E-08
119	5.54E+04	0.0013	2.69E-08
102	6.87E+04	0.0016	2.56E-08
101	6.88E+04	0.0013	2.26E-08
106	8.49E+04	0.0018	3.94E-08
112	9.94E+04	0.001	3.26E-08
111	9.95E+04	0.0012	3.56E-08
103	1.41E+05	0.0016	3.86E-08
104	1.41E+05	0.0013	3.80E-08
107	1.84E+05	0.0017	5.92E-08
113	2.10E+05	0.0013	6.30E-08
114	2.10E+05	0.0014	7.42E-08
108	2.84E+05	0.0013	8.50E-08
109	3.83E+05	0.0012	1.17E-07
131	5.29E+05	0.0012	1.23E-07
132	6.19E+05	0.0012	1.21E-07
133	7.12E+05	0.0012	1.37E-07

Table 4. Pristine *Low Dose* coupons.

Coupon ID	Dose [Gy]	Mols H ₂ Generated
120	2.53E+04	8.12E-09
121	5.45E+04	3.05E-08
105	6.87E+04	4.94E-08
122	9.85E+04	4.79E-08
115	9.94E+04	6.12E-08
123	1.51E+05	6.41E-08
124	2.47E+05	1.15E-07
110	2.84E+05	1.36E-07
125	3.43E+05	1.30E-07

Table 5. Heated pristine *Low Dose* coupons.

Coupon ID	Dose [Gy]	Mols H ₂ Generated	Thermal Treatment
126	6.70E+04	4.41E-08	RT
127	6.70E+04	2.73E-08	200°C
128	6.70E+04	2.62E-08	200°C
129	6.70E+04	1.22E-08	350°C
130	6.70E+04	1.45E-08	350°C

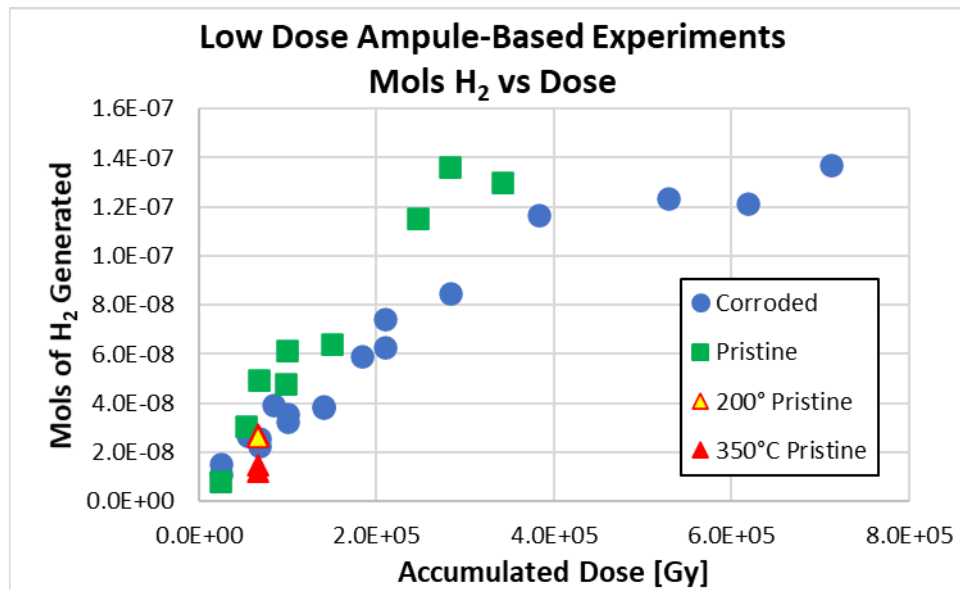


Figure 16. Plot of *Low Dose* coupon H₂ measurements.

The measured radiolytic H₂ generation rate (i.e., the slope of the mols H₂ vs. absorbed gamma dose curve) from pre-corroded coupons appears to decrease with increasing cumulative dose above 400 kGy after an initial linear trend, though it is unclear whether the net H₂ concentration has reached an equilibrium as of 700 kGy. Notably, the pristine coupons generated equal to or greater H₂ yields compared to corroded coupons over the evaluated dose range. This finding confirms that, at least at relatively low absorbed doses,

the physisorbed water contribution to net H₂ generation is significant, and that the rates of generation do not scale linearly with oxyhydroxide mass. Note, however, that the amount of physisorbed water is likely to increase commensurately with oxyhydroxide volume due to increased surface area for adsorption, particularly if the oxyhydroxide morphology is porous, so increasing oxyhydroxide loading could potentially further increase the radiolytic H₂ generation rate.

Five pristine coupons (#126-#130, **Table 5**) were designated to investigate whether elevated temperatures would remove physisorbed moisture from the coupon and therefore reduce H₂ generation to zero which would be postulated for a coupon with neither physisorbed nor chemisorbed water content. Four coupons were heated at either 200 °C or 350 °C for 4 hours in an open-to-air furnace, with one control coupon receiving no heat treatment. The heated coupons were briefly exposed to ambient air for between 5 and 10 minutes prior to being blanketed in dry argon within the Schlenk line. The measured H₂ concentrations indicated a clear difference between the three heat treatments, with coupons heated to 200 °C and 350 °C respectively averaging 40% and 70% less H₂ yield compared to the unheated coupon. The coupons dried to 350 °C still yielded non-zero H₂, but it is currently unclear whether water remained even after the 350 °C thermal treatment or whether this indicates “re-wetting” during the brief exposure to ambient air between heating and flame-sealing. It is also worth investigating whether the heat treatment may have affixed any physisorbed moisture to the coupon by forming a very thin hydrated oxide layer.

Separate from using elevated temperature to dry coupons, the use of extended vacuum hold times was investigated on multiple coupons in the low-dose regime. Three coupon varieties were examined in this limited-scope vacuum experiment: (i) pristine coupons, (ii) pre-corroded coupons, and (iii) large-plate segments (i.e., the sections cut from the large-plate assemblies described in Section 2.2.1). Coupons were exposed to vacuum for various hold times while connected to the Schlenk line at room temperature, immediately prior to being covered with argon and flame sealed within their ampules. Due to time limitations, irradiations were performed by placing ampules symmetrically around the model 484 irradiator source tubes. This extreme proximity introduces some uncertainty in the measured dosimetry, however, as the nearest Fricke measurement of 31.5 Gy/min was taken a few centimeters above the ampule locations. The axial dose at this location is not expected to vary more than 20%, but because exact dosimetry is not known for these samples, their results should not be compared directly to other results in this report. The vacuum experiment results are given in **Table 6** as a function of the *estimated* dose rate.

Table 6. Effect of vacuum hold time on radiolytic H₂ generation.

Coupon Type (condition)	Hours Under Vacuum	Estimated Dose [Gy]	Mols H ₂ Generated	Mols of H ₂ per Gy	Avg. Mol H ₂ / Gy
Pristine (No surface treatment)	0	2.35E+05	9.36E-08	3.99E-13	3.91E-13
		3.55E+05	1.36E-07	3.83E-13	
Large Plate (RT water for 41 days)	12	2.35E+05	7.51E-08	3.20E-13	2.96E-13
		3.55E+05	9.67E-08	2.72E-13	
Large Plate (RT water for 41 days)	0	2.35E+05	8.75E-08	3.73E-13	3.93E-13
		3.55E+05	1.47E-07	4.13E-13	
Large Plate (RT water for 41 days)	12	2.35E+05	4.88E-08	2.08E-13	1.88E-13
		3.55E+05	5.94E-08	1.67E-13	
Corroded (185°C water for 18hr)	4	2.35E+05	2.37E-08	1.01E-13	1.12E-13
		2.35E+05	2.90E-08	1.23E-13	
Corroded (185°C water for 18hr)	72	2.35E+05	3.33E-09	1.42E-14	2.09E-14
		2.35E+05	6.48E-09	2.76E-14	

In contrast to thermal drying, vacuum drying at room temperature should not decompose any existing hydroxide such as gibbsite or bayerite. The reduction in measured H₂ concentrations observed with increasing vacuum hold times further highlights the significance of the physisorbed water contribution to

radiolytic H₂ yield in the low-dose regime. Interestingly, the effect of drying via vacuum appears to be less significant for pristine coupons, which only saw an average of 24% reduction in H₂ generation from a 12-hour vacuum hold time, compared to the bayerite-bearing large-plate coupons which experienced a 52% reduction in H₂ generation. This was observed despite the fact that the physisorbed water expected to be affected by vacuum drying was the only expected radiolytic source on the pristine coupons. A direct comparison between the high-temperature-corrosion coupons with 0 and 12 hour vacuum hold times is unavailable; however, a remarkable 81% reduction in H₂ generation is observed between 4 and 72 hours of vacuum hold time. While these large relative drops in radiolytic H₂ measurements are significant, it remains to be seen whether their trends will hold out at high doses, at which point chemisorbed water contributions may dominate the rate of generation regardless of initial physisorbed water inventory.

3.2 High Dose Ampule-Based Experimental Results

The *High Dose* ampule-based experiments were targeted at a few, individual cumulative dose values beyond those obtained in the original *Low Dose* study. The objective was to verify the existence of H₂ gas equilibration concentrations and to investigate those concentration levels' sensitivity to factors such as starting oxyhydroxide inventory and thermal drying treatments.

Radiolytic H₂ measurements from the *Low Dose* ampules containing 1/16" thick corroded AA1100 coupons (water immersion at 185 °C for 18 hours) were highly suggestive of an attained equilibrium H₂ concentration in the region of cumulative doses assessed. Duplicate *High Dose* coupon samples were irradiated and sampled at dose points in the range 0.7-1.9 MGy with pre-irradiation drying temperatures of room temperature (i.e., no thermal drying), 150 °C, or 200 °C (all expected to be too low to decompose any of the boehmite film). The calculated moles of H₂ determined from GC measurements of each ampule as well as the coupon pre- and post-corrosion weights are given in **Table 7**. The "*No Drying*" and 200 °C groups each show remarkable consistency in the number of H₂ mols measured regardless of cumulative dose, while the intermediate 150 °C case showed a modest increase in H₂ between 0.7-1.9 MGy. However, the 1.9 MGy samples also possessed significantly higher corrosion weight gain. When normalized by weight gain, all *High Dose* coupon results indicate a relatively flat trend of H₂ concentration with respect to absorbed gamma dose. The steady-state H₂ concentrations for both the 150 °C and 200 °C cases were less than 50% of the baseline case with no thermal drying step. The *High Dose* coupon raw H₂ data is plotted in **Figure 17(top)** along with the data normalized to weight gain in **Figure 18(top)**.

High Dose foil samples were measured at cumulative dose values in the range of 1.1-1.8 MGy. Each of these ampules contained eight 0.01" thick AA1100 foils, identical to the coupons in lateral dimensions, corrosion treatment, and thermal drying temperatures. Measured H₂ concentrations from foil samples increased with increasing absorbed dose for all three drying temperatures, even in this "high dose" regime. The number of moles of H₂ measured in the foil-containing ampules did exceed those measured in the coupon-containing ampules at each comparable condition, but the net H₂ production per unit surface area or per unit weight gain was lower for the undried foils than for the corresponding coupons: the foil ampules had 8 times the sample surface area and approximately 5 times the total corrosion weight gain, but the total H₂ yield from the foils at ~1.2 MGy was less than double that of the corresponding coupon ampules. It is possible that the close packing of foils in the ampules reduced the free surface area sufficiently to subdue radiolytic H₂ generation. Furthermore, since no steady-state concentration was observed for the foil cases, the equilibrium H₂ concentrations for the two sample types cannot yet be quantifiably compared on the basis of aluminum surface area or oxyhydroxide mass. Further testing is advised to eliminate surface area crowding and evaluate H₂ concentrations at high total doses to potentially discover a steady-state value. A reduction in net H₂ production was still observed with increasing drying temperatures, with the trend again becoming more apparent when normalized to weight gain. Measured results are provided in **Table 8** with raw and normalized H₂ values plotted in **Figure 17(middle)** and **Figure 18(middle)**, respectively.

Results from the (bayerite-bearing) large-plate segments taken from the *As-Corroded* and *As-Dried* plate assemblies are given in **Table 9** with raw and normalized values plotted in **Figure 17(bottom)** and **Figure 18(bottom)**, respectively. The pre-corroded weights of each segment are estimated based on the percentage weight gain of the entire plate assembly from which each segment was taken. The segments taken from the *As-Dried* plate show significantly less H₂ compared to the *As-Corroded* segments, despite the former having spent several weeks in ambient conditions after the initial 220 °C treatment with the potential to reabsorb surface moisture.

Table 7. High Dose coupon results.

Drying Condition	ID#	Dose [Gy]	Mols H ₂ Generated	μL H ₂ @ STP	Coupon Weight [g]		Weight Gain [g]	Moles per wt. gain [mols/g]
					pre-corr.	Post-corr.		
No Drying	17	1.18E+06	1.96E-07	4.79	0.9902	0.9924	2.20E-03	8.93E-05
	18	1.18E+06	1.95E-07	4.76	0.9904	0.9926	2.20E-03	8.87E-05
	19	1.85E+06	1.91E-07	4.66	0.9889	0.9908	1.90E-03	1.01E-04
	20	1.85E+06	1.96E-07	4.78	0.9878	0.9901	2.30E-03	8.53E-05
150°C 4hr	21	7.65E+05	8.54E-08	2.08	0.9889	0.9912	2.3E-03	3.71E-05
	22	7.65E+05	9.25E-08	2.25	0.9876	0.9901	2.5E-03	3.70E-05
	23	1.85E+06	1.36E-07	3.30	0.9925	0.9962	3.7E-03	3.66E-05
	24	1.85E+06	1.65E-07	4.03	0.9877	0.9922	4.5E-03	3.67E-05
200°C 4hr	13	7.59E+05	7.95E-08	1.94	0.9932	0.9954	2.2E-03	3.61E-05
	14	7.59E+05	8.98E-08	2.19	0.9904	0.9922	1.8E-03	4.99E-05
	15	1.12E+06	8.95E-08	2.18	0.9867	0.9890	2.3E-03	3.89E-05
	16	1.12E+06	8.52E-08	2.07	0.9883	0.9903	2.0E-03	4.26E-05

Table 8. High Dose foil results.

Drying Condition	ID#	Dose [Gy]	Mols H ₂ Generated	μL H ₂ @ STP	Coupon Weight [g]		Weight Gain [g]	Moles per wt. gain [mols/g]
					pre-corr.	Post-corr.		
No Drying	1	1.13E+06	3.40E-07	8.29	1.2964	1.3069	1.05E-02	3.24E-05
	2	1.13E+06	3.41E-07	8.31	1.3194	1.3325	1.31E-02	2.60E-05
	7	1.13E+06	2.29E-07	5.59	1.2914	1.3010	9.60E-03	2.39E-05
	3	1.77E+06	4.57E-07	11.14	1.2724	1.2817	9.30E-03	4.92E-05
	4	1.77E+06	5.16E-07	12.57	1.2980	1.3072	9.20E-03	5.61E-05
	6	1.77E+06	4.85E-07	11.82	1.2927	1.3023	9.60E-03	5.06E-05
150°C 4 hr	27	1.20E+06	3.06E-07	7.46	1.2955	1.3085	1.30E-02	2.36E-05
	28	1.79E+06	5.80E-07	14.14	1.2946	1.3086	1.40E-02	4.15E-05
200°C 4hr	25	1.20E+06	2.32E-07	5.66	1.2904	1.3028	1.24E-02	1.87E-05
	26	1.74E+06	4.15E-07	10.10	1.3000	1.3139	1.39E-02	2.98E-05

Table 9. Large Plate segment results.

Drying Condition	ID#	Dose [Gy]	Mols H ₂ Generated	μL H ₂ @ STP	Coupon Weight [g]		Weight Gain [g]	Moles per wt. gain [mols/g]
					Est. pre-corr.	post-corr.		
As Corroded	Lg1	1.13E+06	5.55E-07	13.53	0.9076	0.9157	8.08E-03	6.88E-05
	Lg2	1.13E+06	4.30E-07	10.47	0.8743	0.8821	7.78E-03	5.53E-05
	Lg3	1.77E+06	5.51E-07	13.43	0.7740	0.7809	6.89E-03	8.00E-05
	Lg4	1.77E+06	5.93E-07	14.44	0.8251	0.8324	7.34E-03	8.07E-05
220°C 4hr	LD1	1.21E+06	1.74E-07	4.23	0.7921	0.7992	7.05E-03	2.46E-05
	LD2	1.21E+06	2.41E-07	5.87	0.8504	0.8580	7.57E-03	3.19E-05

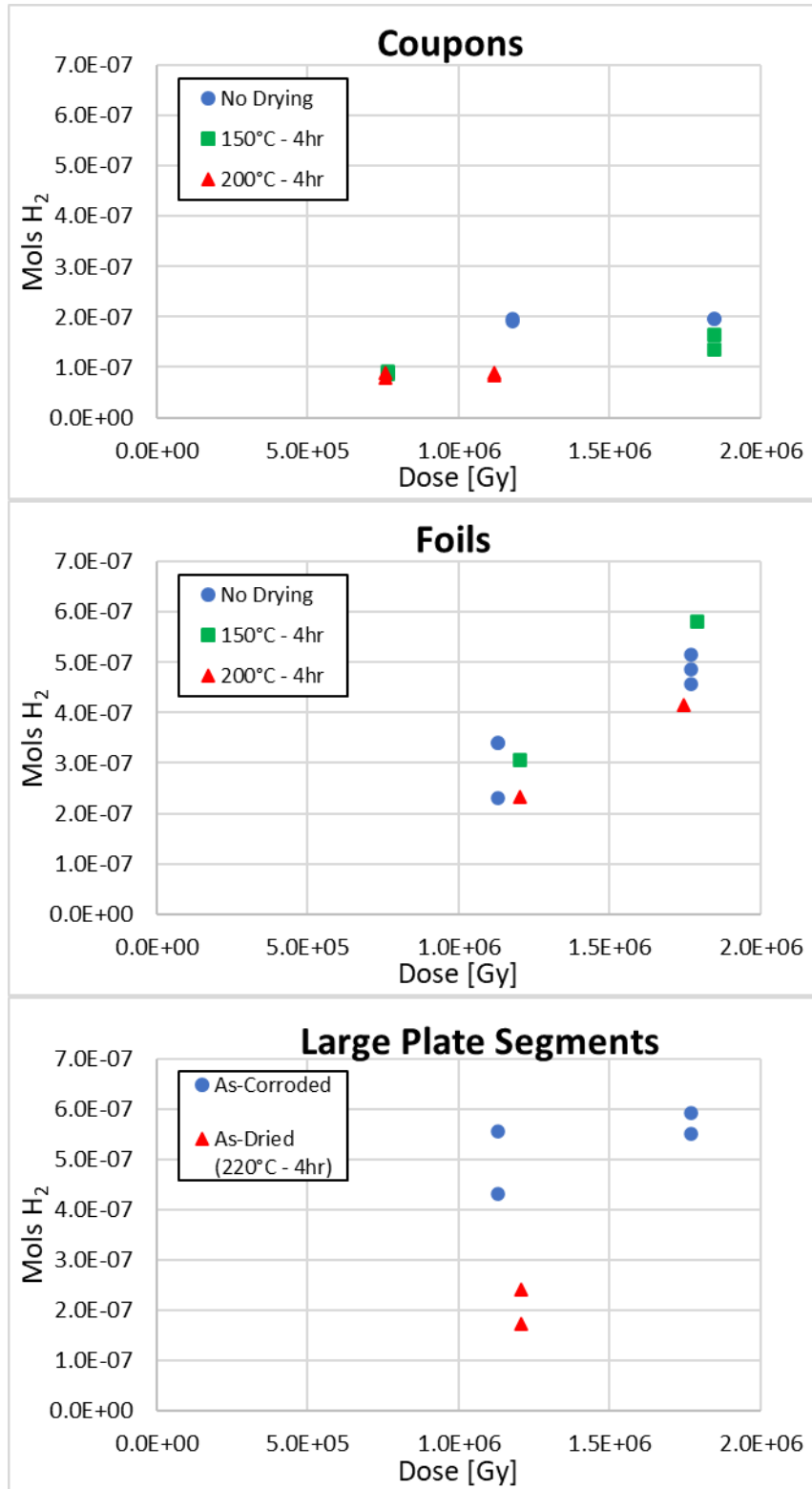


Figure 17. Total moles of H₂ generated as a function of absorbed dose and drying temperature.

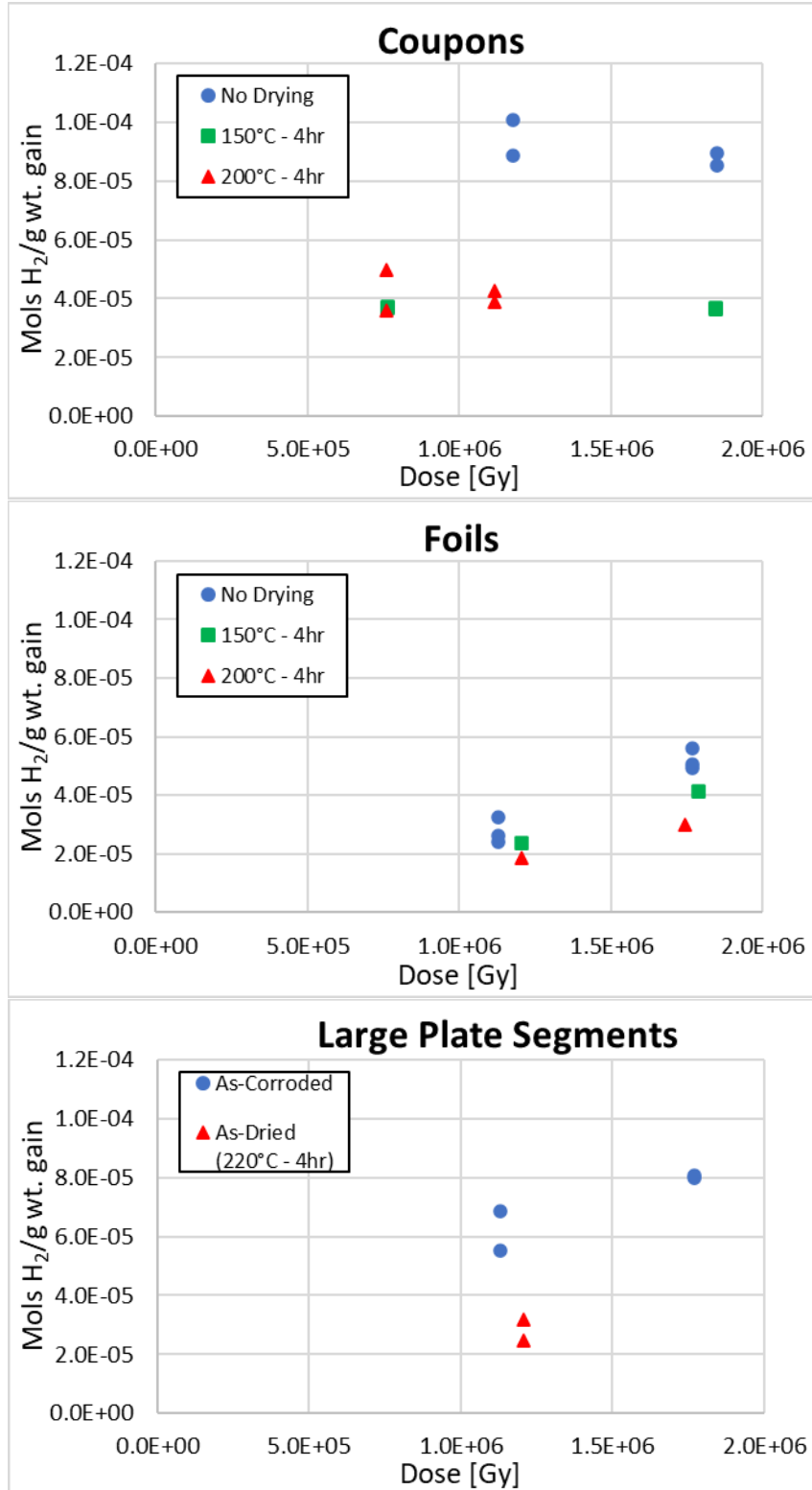


Figure 18. Moles of H₂ generated per gram of corrosion weight gain as a function of absorbed dose and drying temperature.

Four batches of *ASNF Scrap* samples were created by shearing pieces from the bulk scrap small enough to fit within the glass ampules. Two batches (USH1 & USH2) comprised material from the USH while the other two batches (Mk16B1 & Mk16B2) came from two unique areas of the Mk16B. The Mk16B1 batch featured a collection of heavily corroded pieces with visibly thick white oxide. Mk16B2 contained pieces typical of the majority of the Mk16B scrap surface condition and is expected to better match the material characterized previously [7]. The sealed ampules of *ASNF Scrap* batches are shown in **Figure 19**. The *ASNF Scrap* material does not have a known pre-corroded weight since its (oxy)hydroxide was formed during its service history rather than in-lab, and therefore its results cannot be directly compared against lab-grown radiolysis coupons on a per-mass-gain basis. Furthermore, since each scrap batch has different surface areas and potential differences in oxide morphology, it is unwise to directly compare between batches 1 and 2. Each batch was initially irradiated to 0.8 MGy before being measured for H₂ concentration. The batches were then heated in a pre-heated oven at 100 °C for 4 hours before being resealed and re-irradiated to 0.8 MGy. The process was repeated again for a drying temperature of 200 °C. Results from each successive sampling are given in **Table 10** and **Figure 20**.



Figure 19. Sealed ampules containing ASNF Scrap pieces. From left to right, USH1, USH2, Mk16B1, Mk16B2, argon blank.

Table 10. ASNF scrap radiolysis results.

Batch#	Mols H ₂ Generated at 0.8 MGy		
	No Drying	100°C - 4hr	200°C - 4hr
USH1	1.29E-07	1.78E-07	1.19E-07
USH2	1.36E-07	1.97E-07	1.08E-07
Mk16B1	9.42E-06	6.77E-06	2.43E-06
Mk16B2	1.59E-06	1.43E-06	5.49E-07

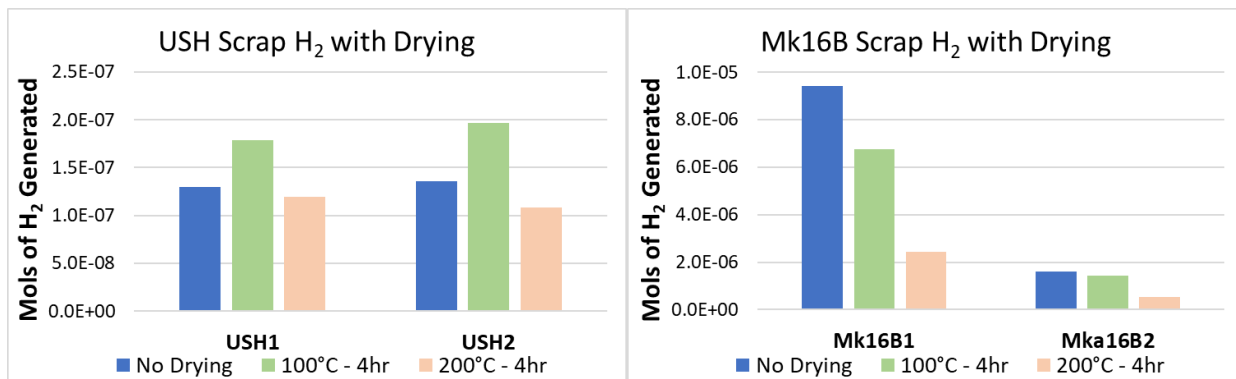


Figure 20. Moles of H₂ generated at 0.8 MGy for ASNF scrap as a function of drying temperature.

A large difference in radiolytic H₂ yield at 0.8 MGy can be seen between the USH and Mk16B, and between the two batches of Mk16B. The heavily corroded batch Mk16B1 produced the largest quantity of H₂ (the undried Mk16B1 yield was ~6 times that of the undried Mk16B2 and ~70 times that of either USH batch). The radiolytic H₂ concentrations measured from the Mk16B pieces decreased with each successive drying temperature evaluated, with the Mk16B1 batch reducing the most dramatically by 75%. The USH batches showed very little impact from drying and even a slight increase in H₂ yield following the 100 °C treatment in both batches, for reasons that are currently unknown.

3.3 Large-Plate Experimental Results

The cumulative moles of H₂ generated by the large-plate assemblies in each vessel have been calculated as a function of their reported absorbed dose. Once again, the dose rate varied across each plate assembly, but the two assemblies were symmetrically situated in the irradiator, and therefore each received the same average dose rate. Gas samples were taken routinely from the sealed vacuum vessels and analyzed for moles of H₂ present in the vessel and manifold using the known volumes and pressures of each. Moles of H₂ removed from the vessels from previous samples are included in the reported total moles generated at each successive sampling point.

Results are tabulated in **Tables 11** and **12** for the *As-Corroded* and *As-Dried* assemblies, respectively, and plotted in **Figure 21**. The H₂ generation rate for both the *As-Corroded* and *As-Dried* assemblies decreased with increasing absorbed gamma dose, as previously observed for the *Low Dose* results in **Figure 16**. A dramatic reduction in both initial H₂ generation rate and H₂ yield is observed for the *As-Dried* assembly compared to the *As-Corroded* assembly, with the *As-Corroded* H₂ yield being more than three times that of the *As-Dried* yield at 2 MGy. In addition, the *As-Dried* assembly yield showed a longer initial delay before measurable H₂ was observed and appeared to approach a plateau/equilibrium H₂ concentration, while the *As-Corroded* H₂ yield continued to climb. When assessing the impact of drying, it should be noted that the predominant (oxy)hydroxide on the *As-Corroded* assembly was bayerite (as opposed to boehmite on the coupon samples corroded at 185 °C), which was partly converted to boehmite by the 220 °C drying process. Therefore, the drying process here removed both physi- and chemisorbed water.

Table 11. *As-Corroded* large plate results.

Dose [Gy]	Pressure [psia]	H ₂ ppm	Total Mols Produced
0.00E+00	23.56	0	0.00E+00
3.21E+04	23.12	299	9.96E-06
6.77E+04	22.67	551	1.82E-05
1.44E+05	22.16	1056	3.42E-05
2.26E+05	21.75	1518	4.87E-05
2.97E+05	21.41	1811	5.80E-05
3.79E+05	20.80	2208	6.94E-05
4.62E+05	20.36	2557	7.95E-05
5.44E+05	20.02	3035	9.35E-05
7.07E+05	19.68	3625	1.10E-04
8.36E+05	18.89	4149	1.23E-04
1.05E+06	18.28	4724	1.36E-04
1.32E+06	18.07	5946	1.69E-04
1.95E+06	17.80	7940	2.18E-04

Table 12. *As-Dried* large plate results.

Dose [Gy]	Pressure [psia]	H ₂ ppm	Total Mols Produced
0.00E+00	24.45	0	0.00E+00
3.58E+04	23.93	0	0.00E+00
7.12E+04	23.42	0	0.00E+00
1.53E+05	22.78	269	8.83E-06
2.35E+05	22.30	382	1.24E-05
3.18E+05	21.86	481	1.56E-05
4.80E+05	21.48	672	2.15E-05
6.13E+05	21.04	805	2.55E-05
8.24E+05	20.36	1001	3.09E-05
1.64E+06	19.70	1895	5.59E-05
2.32E+06	19.23	2239	6.52E-05
2.45E+06	18.72	2275	6.58E-05

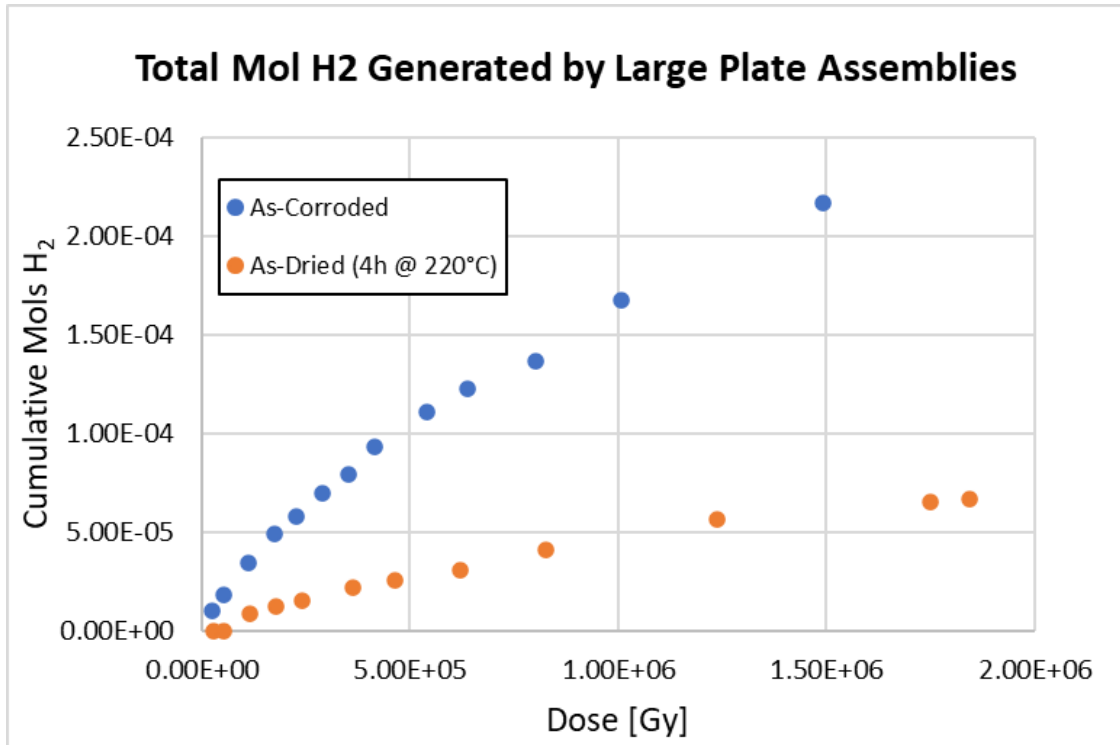


Figure 21. H₂ yields from As-Corroded and As-Dried large-plate assemblies.

4.0 Conclusion

The results from sealed-system aluminum surface radiolysis experiments reported herein have led to several empirical observations from which the following conclusions may be derived regarding radiolytic H₂ generation rates and their dependence on accumulated dose, initial oxyhydroxide inventory, thermal drying, and vacuum drying treatments.

- Within the *Low Dose* regime evaluated (e.g., <0.4 MGy), pristine coupons with nominally no oxyhydroxide content displayed similar or higher H₂ yields compared to corroded (i.e., boehmite-bearing) coupons, suggesting that physisorbed water was the primary source of radiolytic H₂ under these conditions. However, measured H₂ generation totals from the Mk16B1 scrap sample at 0.8 MGy were nearly two orders of magnitude higher than either the pristine or corroded coupon samples at comparable doses. The Mk16B1 scrap contained exceptional quantities of visible corrosion product, including trihydroxides, and therefore certainly possessed more chemisorbed water than the lab-grown counterparts, but it is not known whether the radiolytic hydrogen contribution from the scrap sample is primarily attributable to that chemisorbed water or the physisorbed water. It is anticipated that physisorbed water would increase with increasing oxyhydroxide mass due to increased surface area, particularly for porous corrosion product such as observed on Mk16B1.
- An investigation into the effect of the total aluminum surface area on H₂ generation rates was accomplished by comparing coupon samples to foil samples with 8 times total surface area. While the ampules containing coupons appeared to reach an equilibrium H₂ concentration around 1.0 MGy, the foils were still generating H₂ at a linear rate up to the highest measured dose of 1.77 MGy. The higher total H₂ yield in the foil-containing ampules and the lower values for dried versus undried coupons confirms that the apparent steady-state concentration reached at high dose depends on the sample conditions. The rate of the foils' H₂ generation was less than twice the generation rate initially observed for pristine and corroded coupons despite having 8 times the surface area and 5 times the average post-corrosion weight gain. It is postulated that the rate of H₂ generation

from the foils was subdued due to the fact that many of the foils' surfaces were in direct contact with each other. This surface crowding may have promoted more recombination of radiolytic species and reduced net H₂ formation rates. A revised experiment to identify potential equilibria concentrations for various surface area samples is needed to establish whether the roll-over in net H₂ generation rate is a function of initial water inventory, competing radiolytic reactions affected by partial H₂ pressure, or a combination of both.

- Drying processes, both thermal and vacuum drying, were shown to significantly reduce the H₂ generation rate under gamma irradiation in the low-dose regime as well as the observed equilibrium H₂ concentrations in the *High Dose* regime.
- An extended vacuum drying step of 12 hours significantly reduced the H₂ generation in ampule-based experiments compared to samples experiencing only the standard, short vacuum holds during the Schlenk line conditioning. The reduction in H₂ yield was observed for both pristine samples expected to hold only physisorbed water and for corroded aluminum samples expected to contain both physi- and chemisorbed water. In the limited testing scope, the undried pristine and bayerite-coated samples had very similar H₂ yield, and the reduction in yield for samples with a bayerite layer was almost twice that for pristine coupons. An (oxy)hydroxide layer is expected to increase the microscopic surface area and thus the physisorbed water inventory compared to a pristine sample, and the presence of a bayerite or boehmite layer may affect how strongly physisorbed water adheres to the surface. (Oxy)hydroxide layers may also impact the radiation energy transfer rates and distribution between the sample and the physisorbed water as compared to a pristine aluminum coupon with a relatively thin, compact alumina surface.
- Thermal drying was shown to significantly reduce the H₂ yield from pristine coupons at low dose, with ~40% and ~70% reduction for coupons heated to 200 °C and 350 °C, respectively, for 4 hours. The H₂ yield was not reduced to zero by the thermal drying, suggesting that either some strongly adsorbed water remained despite the heating or that re-adsorption occurred rapidly during the short exposure to ambient air between coupon drying and ampule sealing.
- Thermal drying of a large plate assembly with a bayerite surface layer at a temperature high enough to partially dehydrate the bayerite (220 °C) reduced the H₂ yield at ~2 MGy by ~70%. The reduction in final H₂ yield may be even larger, since the *As-Dried* assembly appeared to be approaching a plateau while the *As-Corroded* H₂ yield continued to climb. Note that both large-plate assemblies experienced a 12-hour vacuum hold prior to irradiation, so even the *As-Corroded* assembly most likely had a significant amount of water removed.
- Thermal drying of the ASNF scrap produced ambiguous results. The samples were dried to temperatures expected to remove only physisorbed water without decomposing the oxyhydroxide. The H₂ yield from USH samples showed little change from different drying temperatures and included an unexpected, slight increase in yield after drying to 100 °C. The Mk16B samples, which featured significantly more visible corrosion product and a commensurately large H₂ yield without thermal drying treatment, exhibited a pronounced reduction in H₂ yield with increasing drying temperature, up to 75% reduction for the heavily corroded Mk16B1 sample at 200 °C.

It is evident from these results that radiolytic H₂ generation rates from hydrated aluminum surfaces and the steady state concentrations of H₂ achieved in a sealed system are affected by thermal drying treatments and prolonged exposure to vacuum. This is likely attributable to a reduction in the total water inventory present on the aluminum surface. While the results discussed here do indicate a significant contribution to the radiolytic H₂ generation from physisorbed water, radiolytic H₂ production persists following vacuum and thermal treatments intended to remove free and physisorbed water.

Additional investigation is recommended to identify bounding equilibrium H₂ concentrations using high dose rates and online, sequential gas sampling similar to that described in the large plate experiments. This method would allow comparison between the relatively constant net H₂ generation rate in the low dose regime against the ultimate steady state concentrations for a variety of variables such as drying treatment and aluminum surface area. This comparison could drastically improve or validate the accuracy of predictive radiolytic models for sealed ASNf storage containers. As it is still unclear whether the observed reduction in net H₂ generation is due to primarily to depletion of inventory or competing back reactions with other radiolytic species, it is proposed that sealed systems that have reached steady state H₂ concentrations be evacuated and refilled with cover gas prior to continuing irradiation. If further H₂ generations is observed, then it may be inferred that the original roll-over in H₂ concentration was not due entirely to depletion of the initial water inventory. Further insight into the mechanism behind the H₂ concentration roll-over can be gained by artificially increasing the partial pressure of H₂ in the sealed system in the early low dose regime and observing the effect, if any, on the ordinarily constant generation rate typically observed at these doses. The ability to confidently predict or at least bound steady state H₂ concentrations in sealed storage based on initial generation rates would dramatically increase the value of dry cask monitoring systems and potentially allow for the determination of a cask's H₂ end state before it even leaves the wet storage facility.

5.0 References

- [1] DOE. (2017b). Aluminum-Clad Spent Nuclear Fuel: Technical Considerations and Challenges for Extended (>50 Years) Dry Storage (DOE/ID RPT #: 1575).
- [2] M. J. Connolly, J. J. Jarrell, *Aluminum Clad Spent Nuclear Fuel Long Term Dry Storage Technical Issues Action Plan – Technical and Engineering Activities*, Idaho National Laboratory, INL/EXT-17-43908, 2017.
- [3] E. H. Parker-Quaife, G.P. Horne, C. R. Heathman, C. G. Verst, and P. R. Zalupski, *Radiation-Induced Molecular Hydrogen Gas Generation by Pre-Corroded Aluminum Alloy 1100*, Idaho National Laboratory, INL/EXT-19-55202 Rev. 1, 2019.
- [4] H. Lee, Y. Jeon, S. U. Lee, D. Sohn, *Temperature Effect on Synthesis of Gibbsite and Boehmite*, Department of Chemistry and Research Institute of Natural Sciences, CL-130665, 2013.
- [5] T.J. Ruff, R.K. Toghiani, L. T. Smith, J.S. Lindner, *Studies on the Gibbsite to Boehmite Transition*, Separation Science and Technology, 43:9-10 2887-2899, 2008.
- [6] *Corrosion of Research Reactor Aluminum Clad Spent Fuel in Water*, International Atomic Energy Agency, IAEA-TECDOC-1637, 2010.
- [7] L. Olson, C. Verst, A. d’Entremont, R. Fuentes, R. Sindelar, *Characterization of Oxide Films on Aluminum Materials following Reactor Exposure and Wet Storage in the SRS L-Basin*, Savannah River National Laboratory, SRNL-STI-2019-00058, 2019.
- [8] G. P. Horne, E. H. Parker-Quaife, C. G. Verst, C. L. Crawford, R. L. Sindelar, *Milestone 2.6 Complete Round-Robin Hydrogen Gas Analysis Capability Comparison*, Idaho National Laboratory, INL/EXT-20-00810, Rev. 1, 202